Testing *ab initio* nuclear structure in neutron-rich nuclei: Lifetime measurements of second 2⁺ state in ¹⁶C and ²⁰O

M. Ciemała,[1,*] S. Ziliani,[2,3] F. C. L. Crespi,[2,3] S. Leoni,[2,3,†] B. Fornal,[1,‡] A. Maj,[1] P. Bednarczyk,[1] G. Benzoni,[3] A. Bracco,[2,3] C. Boiano,[3] S. Bottoni,[2,3] S. Brambilla,[3] M. Bast,[4] M. Beckers,[4] T. Braunroth,[4] F. Camera,[2,3] N. Cieplicka-Oryńczak,[1] E. Clément,[5] S. Coelli,[3] O. Dorvaux,[6] S. Erturk,[7] G. de France,[5] C. Fransen,[4] A. Goldkuhle,[4] J. Grębosz,[1] M. N. Harakeh,[8] Ł. W. Iskra,[1,3] B. Jacquot,[5] A. Karpov,[9] M. Kicińska-Habior,[10] Y. Kim,[5] M. Kmiecik,[1] A. Lemasson,[5] S. M. Lenzi,[11,12] M. Lewitowicz,[5] H. Li,[5] I. Matea,[13] K. Mazurek,[1] C. Michelagnoli,[14] M. Matejska-Minda,[15,1] B. Million,[3] C. Müller-Gatermann,[4] V. Nanal,[16] P. Napiorkowski,[15] D. R. Napoli,[17] R. Palit,[16] M. Rejmund,[5] Ch. Schmitt,[6] M. Stanoiu,[18] I. Stefan,[13] E. Vardaci,[19] B. Wasilewska,[1] O. Wieland,[3] M. Zieblinski,[1] M. Zielińska,[20] A. Ataç,[21] D. Barrientos,[22] B. Birkenbach,[4] A. J. Boston,[23] B. Cederwall,[21] L. Charles,[6] J. Collado,[24] D. M. Cullen,[25] P. Désesquelles,[26] C. Domingo-Pardo,[27] J. Dudouet,[28] J. Eberth,[4] V. González,[24] J. Goupil,[5] L. J. Harkness-Brennan,[23] H. Hess,[4] D. S. Judson,[23] A. Jungclaus,[29] W. Korten,[20] M. Labiche,[30] A. Lefevre,[5] R. Menegazzo,[11] D. Mengoni,[11,12] J. Nyberg,[31] R. M. Perez-Vidal,[27] Zs. Podolyak,[32] A. Pullia,[2,3] F. Recchia,[11,12] P. Reiter,[4] F. Saillant,[5] M. D. Salsac,[20] E. Sanchis,[24] O. Stezowski,[28] Ch. Theisen,[20] J. J. Valiente-Dobón,[17] J. D. Holt,[33,34] J. Menéndez,[35,36] A. Schwenk,[37,38,39] and J. Simonis[40]

[1]*Institute of Nuclear Physics, PAN, 31-342 Kraków, Poland*
[2]*Dipartimento di Fisica, Università degli Studi di Milano, I-20133 Milano, Italy*
[3]*INFN Sezione di Milano, via Celoria 16, 20133, Milano, Italy*
[4]*Institut für Kernphysik, Universität zu Köln, 50937 Cologne, Germany*
[5]*GANIL, CEA/DRF-CNRS/IN2P3, Boulevard Henri Becquerel, Boîte Postale 55027, F-14076 Caen, France*
[6]*CNRS/IN2P3, IPHC UMR 7178, F-67037 Strasbourg, France*
[7]*Department of Physics, Science and Art Faculty, Nigde Omer Halisdemir University, Nigde, Turkey*
[8]*KVI-Center for Advanced Radiation Technology, Groningen, The Netherlands*
[9]*FLNR, JINR, 141980 Dubna, Russia*
[10]*Faculty of Physics, University of Warsaw, Warsaw, Poland*
[11]*INFN Sezione di Padova, I-35131 Padova, Italy*
[12]*Dipartimento di Fisica e Astronomia, Università degli Studi di Padova, I-35131 Padova, Italy*
[13]*IPN Orsay Laboratory, Orsay, France*
[14]*Institut Laue-Langevin (ILL), Grenoble, France*
[15]*Heavy Ion Laboratory, University of Warsaw, PL 02-093 Warsaw, Poland*
[16]*Tata Institute of Fundamental Research, Mumbai 400005, India*
[17]*INFN Laboratori Nazionali di Legnaro, I-35020 Legnaro, Italy*
[18]*IFIN-HH, Bucharest, Romania*
[19]*Università degli Studi di Napoli, and INFN Sezione di Napoli, Italy*
[20]*IRFU, CEA/DRF, Centre CEA de Saclay, F-91191 Gif-sur-Yvette Cedex, France*
[21]*Department of Physics, Royal Institute of Technology KTH, SE-10691 Stockholm, Sweden*
[22]*CERN, CH-1211 Geneva 23, Switzerland*
[23]*Oliver Lodge Laboratory, The University of Liverpool, Liverpool L69 7ZE, United Kingdom*
[24]*Departamento de Ingeniería Electrónica, Universitat de Valencia, Burjassot, Valencia, Spain*
[25]*Nuclear Physics Group, Schuster Laboratory, University of Manchester, Manchester M13 9PL, United Kingdom*
[26]*CSNSM, Université Paris-Sud/CNRS-IN2P3, Université Paris-Saclay, Bâtiment 104, F-91405 Orsay Campus, France*
[27]*Instituto de Física Corpuscular, CSIC-Universidad de Valencia, E-46071 Valencia, Spain*
[28]*Université de Lyon 1, CNRS/IN2P3, UMR5822, IPNL, F-69622 Villeurbanne Cedex, France*
[29]*Instituto de Estructura de la Materia, CSIC, Madrid, Spain*
[30]*STFC Daresbury Laboratory, Daresbury, Warrington WA4 4AD, United Kingdom*
[31]*Department of Physics and Astronomy, Uppsala University, SE-75120 Uppsala, Sweden*
[32]*Department of Physics, University of Surrey, Guildford GU2 7XH, United Kingdom*
[33]*TRIUMF, 4004 Wesbrook Mall, Vancouver, British Columbia V6T 2A3, Canada*
[34]*Department of Physics, McGill University, 3600 rue University, Montreal, Québec H3A 2T8, Canada*
[35]*Center for Nuclear Study, University of Tokyo, Tokyo 113-003, Japan*
[36]*Departament de Física Quántica i Astrofísica Martí i Franqués 1, 08028 Barcelona, Spain*
[37]*Institut für Kernphysik, Technische Universität Darmstadt, 64289 Darmstadt, Germany*
[38]*ExtreMe Matter Institute EMMI, GSI Helmholtzzentrum für Schwerionenforschung GmbH, 64291 Darmstadt, Germany*
[39]*Max-Planck-Institut für Kernphysik, Saupfercheckweg 1, 69117 Heidelberg, Germany*
[40]*Institut für Kernphysik and PRISMA Cluster of Excellence, Johannes Gutenberg-Universität Mainz, 55128 Mainz, Germany*

To test the predictive power of *ab initio* nuclear structure theory, the lifetime of the second 2^+ state in neutron-rich ^{20}O, $\tau(2_2^+) = 150^{+80}_{-30}$ fs, and an estimate for the lifetime of the second 2^+ state in ^{16}C have been obtained for the first time. The results were achieved via a novel Monte Carlo technique that allowed us to measure nuclear state lifetimes in the tens-to-hundreds of femtoseconds range by analyzing the Doppler-shifted γ-transition line shapes of products of low-energy transfer and deep-inelastic processes in the reaction ^{18}O (7.0 MeV/u) + ^{181}Ta. The requested sensitivity could only be reached owing to the excellent performances of the Advanced γ-Tracking Array AGATA, coupled to the PARIS scintillator array and to the VAMOS++ magnetic spectrometer. The experimental lifetimes agree with predictions of *ab initio* calculations using two- and three-nucleon interactions, obtained with the valence-space in-medium similarity renormalization group for ^{20}O and with the no-core shell model for ^{16}C. The present measurement shows the power of electromagnetic observables, determined with high-precision γ spectroscopy, to assess the quality of first-principles nuclear structure calculations, complementing common benchmarks based on nuclear energies. The proposed experimental approach will be essential for short lifetime measurements in unexplored regions of the nuclear chart, including *r*-process nuclei, when intense beams, produced by Isotope Separation On-Line (ISOL) techniques, become available.

DOI: 10.1103/PhysRevC.101.021303

Atomic nuclei are composed of protons and neutrons, which, in turn, are systems of quarks and gluons confined via the strong interaction, as described by quantum chromodynamics (QCD). Ideally, one would like to obtain the properties of nuclei solving QCD, but despite recent progress, this is beyond current computational capabilities [1–3]. At the energy and momentum scales relevant for nuclear structure, chiral effective field theory (EFT), an effective theory based on the symmetries of QCD, provides a practical alternative [4–6]. In chiral EFT, the degrees of freedom are nucleons and pions, and nuclear forces are given by a systematic expansion of two-nucleon (NN), three-nucleon (3N), and many-nucleon interactions that include pion exchanges and contact terms.

In recent years, chiral EFT interactions have been combined with *ab initio* approaches that consider all nucleons in the solution of the nuclear many-body problem in studies of midmass nuclei up to tin [7–12]. Theoretical results are typically compared to the simplest experimental observables, namely, binding and excitation energies. First calculations of medium-mass nuclei with chiral NN + 3N interactions predicted correctly the oxygen neutron drip line at ^{24}O [8,13], and later works reproduced well the excitation spectra of neutron-rich oxygen isotopes [8]. In neutron-rich calcium and nickel isotopes, the shell evolution was also satisfactorily predicted [14–16]. Tests of *ab initio* calculations against other observables include charge radii [17,18], β-decay lifetimes [19], and elastic proton scattering off ^{10}C [20]. Electromagnetic (EM) responses have also been studied in selected nuclei

[21–23]. A general agreement between theory and experiment was found.

Electric and magnetic γ decays provide a more demanding complementary test of theoretical approaches. So far, EM decays in light- and medium-mass systems have only been explored in few cases [24–29]. In contrast to energies or β decays, *ab initio* methods do not yet consistently describe all the data related to EM transitions. This calls for precision measurements of EM observables which are sensitive to the details of the calculations. Ideal cases are neutron-rich O and C isotopes. Here, *ab initio* approaches show a strong sensitivity of EM decays to 3N forces which significantly affect the lifetime of selected excited states by changing the wave function composition [30].

In this Rapid Communication, we focus on the lifetime determination of the second 2^+ excitations, 2_2^+, in ^{20}O and ^{16}C nuclei. We confront our results with predictions of the valence-space in-medium similarity renormalization group (VS-IMSRG) and of the no-core shell model (NCSM) of Ref. [30], both including NN and 3N forces. Previous experiments have only set limits on the lifetime of these 2_2^+ states, of the order of a few picoseconds, and provided information on branching ratios in their decays [31–34]. In this Rapid Communication, we aim at a much more stringent test of *ab initio* calculations by measuring the 2_2^+ state lifetimes.

In ^{20}O, the first-excited 2_1^+ state at 1674 keV decays with a lifetime of 10.4(9) ps [35]. The 2_2^+ state, of our interest, located at 4070 keV, was found to decay to the 2_1^+ state with a 72(8)% branch [31], in parallel to the direct ground-state branch for which contradicting $B(E2)$ information is reported from intermediate-energy Coulomb excitation [36,37]. In ^{16}C, the 2_1^+ state at 1762 keV decays with a lifetime of 11.4(10) ps [33], whereas for the 2_2^+ state lifetime only the upper limit of 4 ps is known [32,33]. Theoretical predictions suggest that the lifetimes of these 2_2^+ states are in the tens-to-hundreds of femtoseconds range. This poses an experimental challenge since such neutron-rich systems can only

*Corresponding author: michal.ciemala@ifj.edu.pl

†silvia.leoni@mi.infn.it

‡bogdan.fornal@ifj.edu.pl

be produced, with sizable cross sections, in: (i) relativistic heavy-ion fragmentation, for which the lower limit in lifetime determination is a few hundreds of femtoseconds as shown by Morse *et al.* [38], (ii) low-energy transfer and deep-inelastic reactions, where the complex structure of the product velocity distribution, caused by large energy dissipations [39,40], does not allow to use standard Doppler shift attenuation methods [41].

In this Rapid Communication, we have developed a technique which enables us to access tens-to-hundreds of femtosecond lifetimes in exotic neutron-rich nuclei with low-energy transfer and deep-inelastic heavy-ion reactions—our approach is a significant extension of the Doppler-shift attenuation method to cases without well-defined reaction kinematics. It will be an essential and quite unique tool to determine short lifetimes in nuclei with large neutron excess, including *r*-process nuclei, when intense Isotope Separation On-Line- (ISOL-) type beams [42], currently under development, are available. The novelty of the method relies on the accurate reconstruction of the complex initial velocity distribution of the reaction product excited to a specific nuclear state, including contributions from direct and dissipative processes. The Doppler-shifted γ-transition line shape is then simulated considering the precisely determined detection angle between the γ ray and the reconstructed initial product velocity inside the target. It will be shown that the required sensitivity to the lifetimes could only be achieved by the excellent performances of our integral AGATA + PARIS + VAMOS detection system.

In the present Rapid Communication, ^{16}C and ^{20}O nuclei were populated in both direct transfer and deep-inelastic processes induced by an ^{18}O beam at 126 MeV on a ^{181}Ta target (6.64 mg/cm^2). The beam energy at the center of the target was $\sim$116 MeV, i.e., $\sim$50% above the Coulomb barrier, and projectilelike products had velocities of $v/c \sim 10\%$. The experiment was performed at the Grand Accélérateur National d'Ions Lourds (GANIL) with 31 high-purity Ge detectors of the AGATA array [43,44], coupled to a scintillator array consisting of two large volume (3.5″ × 8″) LaBr$_3$ detectors plus two clusters of the PARIS setup [45], which produced excellent time reference for the reaction. Reaction products were detected in the VAMOS++ spectrometer [46,47], placed at the reaction grazing angle of 45° (opening angle ±6°) with respect to the beam direction and aligned with the center of AGATA. Relative to the VAMOS++ axis, AGATA covered the 115°–175° angular range, whereas the scintillators were placed at 90°. More than 10^7 events were collected requiring coincidences between projectilelike products detected in VAMOS++ and γ rays in AGATA or PARIS. The VAMOS++ setting was optimized to detect ^{20}O within a large velocity range, including quasielastic and deep-inelastic processes. Other products with charge $5 \leqslant Z \leqslant 9$ and mass number $11 \leqslant A \leqslant 21$ were also detected. Identification plots of O and C ions are given in Fig. 1 together with the velocity distributions measured in VAMOS++ for the 2_2^+ states in ^{20}O and ^{16}C. In the case of ^{20}O, the velocity distribution shows a pronounced peak, corresponding to the direct population in a quasielastic process, whereas the tail, extending towards lower velocities, is associated with higher kinetic-energy loss. The
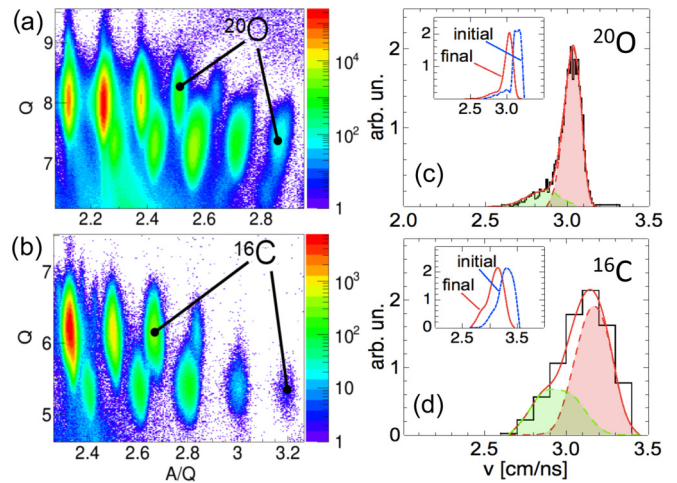

FIG. 1. Left: Identification plots, charge Q versus A/Q for (a) O and (b) C ions, as measured by VAMOS++. Right: velocity distributions measured at the VAMOS++ focal plane (black histograms) in coincidence with $2_2^+ \rightarrow 2_1^+$ transitions of (c) ^{20}O and (d) ^{16}C, detected in AGATA. The solid red lines are simulated final velocity distributions—quasielastic (deep-inelastic) components are given by the red (green) shaded areas. The insets: reconstructed initial (dashed blue lines) and final (solid red lines) product velocities.

velocity distribution is similar in ^{16}C, although with a much larger contribution ($\sim$32%) from dissipative processes.

Portions of γ-ray spectra obtained with AGATA by gating on ^{19}O, ^{20}O, and ^{16}C ions, Doppler corrected considering the product velocity vector measured in VAMOS++, are shown in Fig. 2, panels (a)–(c), respectively. All visible γ rays correspond to known transitions (see level schemes on the right). A closer inspection reveals that some of the peaks are narrow and their energies agree, within uncertainty, with earlier studies. This is the case of transitions from relatively long-lived levels ($\tau > 1$ ps), emitted in flight outside the target as, for example, the 1375- and 2371-keV lines in ^{19}O, the 1674-keV line in ^{20}O, and the 1762-keV peak in ^{16}C [48].

In contrast, other lines, depopulating states with lifetimes shorter than 1 ps, exhibit rather large widths and tails. This indicates that the corresponding γ rays were partly emitted during the stopping process of the reaction product inside the target, i.e., at larger velocity than the one measured in VAMOS++. In these cases, the Doppler-broadened line shape can be used to determine the lifetime of the state.

The Monte Carlo simulation of the Doppler-shifted γ-transition line shapes was performed in three steps [49]. First, we reconstruct, iteratively, the initial product velocity distribution inside the target, associated with the population of a given state (see Fig. 1). The procedure is based on the VAMOS++ measured velocity-angle distribution (the spectrometer response function is considered [47]), the reaction kinematics calculated for the selected state (including direct population and more dissipative processes), a random probability of reaction occurrence over the target thickness, and the slowing-down and straggling processes inside the target from Ziegler *et al.* [50] and Anne *et al.* [51]. Second, we simulate the Doppler-shifted energy measured in AGATA
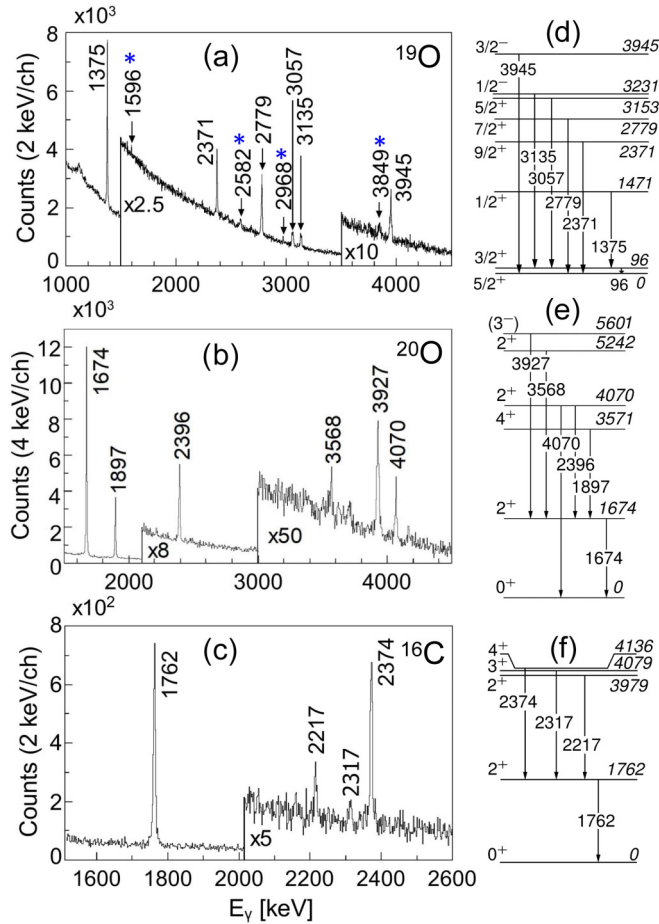
FIG. 2. Left: γ-ray spectra of (a) ^{19}O, (b) ^{20}O, and (c) ^{16}C, as measured by AGATA. Right: Corresponding level schemes of (d) ^{19}O, (e) ^{20}O, and (f) ^{16}C. In (a), the blue stars mark weak transitions of ^{19}O not shown in (d).

for a transition emitted by the moving product nucleus, with lifetime and transition energy as parameters. Here, the angle between the product velocity at the emission point and the γ-ray direction is determined with precision of ~1.5° (i.e., 1° for AGATA and 1° for VAMOS++). Finally, we minimize the χ^2 surface, in lifetime-energy coordinates, by comparing the simulated and experimental transition line shapes for three selected angular ranges (i.e., 120°–140°, 140°–160°, and 160°–180°), simultaneously.

Figures 3(a)–3(c) and 3(d)–3(f) show the 2371- and 2779-keV lines from the decay of the $9/2^+$ and $7/2^+$ states in ^{19}O, with lifetimes of $\tau > 3.5$ ps and $\tau = 92(19)$ fs, respectively [52,53]. In Figs. 3(d)–3(f), the spectra for each angular range are overlaid with the results of the simulations within 1σ uncertainty around the optimum γ energy (E_γ) and lifetime value. The insets show the corresponding χ^2 surface, with the white cross and the solid line indicating the well-localized minimum and the 1σ uncertainty contour. Our final results, $E_\gamma = 2779.0^{+1.0}_{-0.8}$ keV and $\tau = 140^{+50}_{-40}$ fs are in agreement with the literature values, within uncertainties. Figures 3(a)–3(c) display similar analyses for the long-lived ($\tau > 3.5$ ps) 2371-keV line. Here, the χ^2 map shows a valley at $E_\gamma =$

$2370.6^{+0.5}_{-0.3}$ keV, extending from 400 fs towards higher values without a localized minimum. Both ^{19}O results validate our novel Monte Carlo analysis.

We now turn to the lifetime of the 2^+_2 states in ^{20}O and ^{16}C. Figures 3(g)–3(i) refer to the $2^+_2 \rightarrow 2^+_1$ decay in ^{20}O. A well-defined minimum is found on the χ^2 surface, yielding the values $E_\gamma = 2394.6^{+1.0}_{-1.0}$ keV and $\tau = 150^{+80}_{-30}$ fs. We note that the γ-ray energy agrees with the most precise value reported in literature, i.e., $E_\gamma = 2396(1)$ keV [31], whereas the present determination of the lifetime is the first obtained, thus far. For the $2^+_2 \rightarrow 2^+_1$ decay, considering its 79(5)% branching ratio, here determined, one gets a partial lifetime of 190^{+102}_{-40} fs. We stress that the above results rely on the AGATA excellent position resolution of the first γ interaction point, determined with the combined use of pulse shape analysis [54,55] and the Orsay forward tracking algorithm [56]. Defining the γ direction from the front segment centers only, as in the case of conventional Ge arrays, gives χ^2 minima with much larger uncertainty [dashed lines in the insets of Figs. 3(d)–3(g)], making meaningless a comparison with theory.

Figures 3(j) and 3(k) report the analysis of the 2^+_2 state in ^{16}C, performed on the γ-ray spectrum integrated over the entire angular range, i.e., 120°–180°, due to the limited statistics. As a consequence, the ^{16}C χ^2 map, shown in Fig. 3(j), displays a wide valley, resulting in a very limited sensitivity when $E_\gamma < 2216$ keV. For $2^+_2 \rightarrow 2^+_1$ transition energies $E_\gamma > 2216$ keV, the procedure provides a more definite value, which would indicate a lifetime of $\tau < 180$ fs. Considering the most precise energy measurement $E_\gamma = 2217(2)$ keV [33], there is a 78% probability for this scenario.

We performed calculations for ^{20}O by employing chiral NN interactions based on Ref. [57], and 3N interactions fitted on top, considering only few-body systems up to ^{4}He. First, the many-body perturbation theory (MBPT) valence-shell interactions from Ref. [8] were employed with an ^{16}O core. NN and normal-ordered 3N interactions are included up to third order, neglecting residual 3N interactions. Effective operators are used to calculate EM transitions [58,59]. The shell-model diagonalizations were performed with the code ANTOINE [60]. The MBPT results reproduce well the $2^+_1 \rightarrow 0^+$ lifetime in ^{20}O ($\tau = 11.7$ ps versus the experimental $\tau = 10.5(4)$ ps [35]), and this agreement does not depend significantly on the inclusion of 3N interactions. In turn, as shown in Fig. 4, the calculated partial lifetime of the $2^+_2 \rightarrow 2^+_1$ decay, $\tau = 275$ fs (the dashed blue line), agrees well with the present measurement only when 3N interactions are considered [$B(M1) = 0.015\mu^2_N$, $B(E2) = 0.051$ e^2fm^4, taking the experimental transition energy]. When they are neglected, the $2^+_2 \rightarrow 2^+_1$ partial lifetime is about 60% longer (the dashed green line), and the energy of the 2^+_2 state is more than 1 MeV lower (see also Ref. [8]). This change is driven by the dominant $(d_{5/2})^3(s_{1/2})^1$ configuration, which is mostly missing in the NN calculation.

Second, we performed *ab initio* calculations with the VS-IMSRG [8,12,61–63], based on the NN + 3N interaction labeled EM1.8/2.0 in Ref. [64]. The treatment of 3N interactions improves that of the MBPT by including approximately the interactions between valence nucleons [63]. In
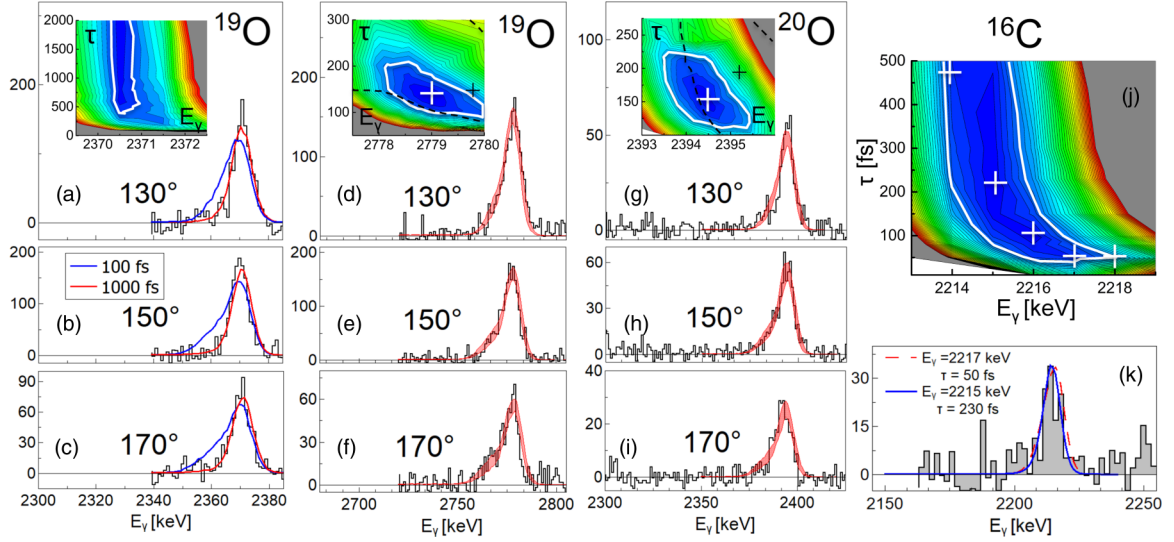
FIG. 3. Panels (a)–(c), (d)–(f), and (g)–(i): 2371-, 2779-, and 2396-keV γ rays from the long-lived ($\tau > 3.5$ ps) $9/2^+$ state in ^{19}O and the $7/2^+$ and the 2_2^+ states in ^{19}O and ^{20}O, respectively, as measured by AGATA (precision < 4 mm) in the angular ranges of $130° \pm 10°$, $150° \pm 10°$, and $170° \pm 10°$. In (d)–(f) and (g)–(i), simulated spectra (shaded bands) are calculated on the basis of the global χ^2 lifetime-energy surface (see the corresponding insets) with 1σ uncertainty (white contour line) around the optimum γ-energy (E_γ) and lifetime (τ) values (white cross). The black crosses and dashed lines indicate the χ^2 minimum and 1σ uncertainty for γ-detection angles defined by the AGATA front segment centers (precision $\sim$20 mm). In (a)–(c), simulated spectra for $\tau = 100$ and 1000 fs (blue and red lines, respectively) are shown to demonstrate the absence of broadening and tails for decays from long-lived states. Panel (j): χ^2 surface for the ^{16}C $2_2^+ \rightarrow 2_1^+$ transition. Panel (k): ^{16}C $2_2^+ \rightarrow 2_1^+$ transition measured over the full AGATA angular range (histogram), compared with simulated spectra relative to the minimum of the χ^2 map, for $E_\gamma = 2215$ keV ($\tau = 230$ fs) and $E_\gamma = 2217$ keV ($\tau = 50$ fs).

addition, we decouple valence-space operators consistent with the Hamiltonian as in Refs. [26,65], avoiding the use of effective charges or g factors and producing effective two-body EM operators. In the IMSRG(2) approximation used here, all operators are truncated at the two-body level, which leads to reduced $B(E2)$ values as discussed in Ref. [26].
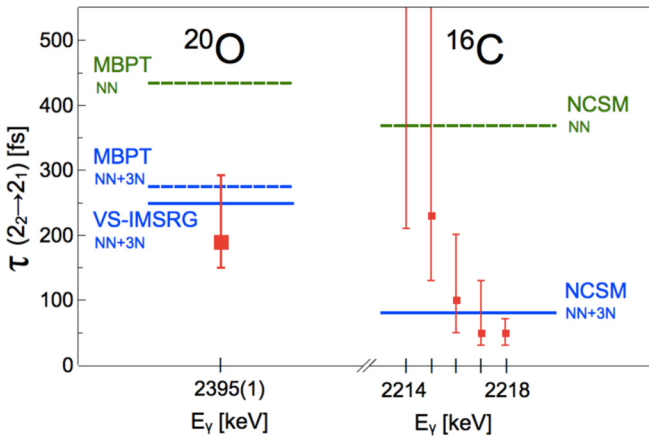

FIG. 4. Partial lifetime for $2_2^+ \rightarrow 2_1^+$ decays. Left: ^{20}O, experiment (symbol) compared to MBPT (dashed lines, with and without 3N interactions), and *ab initio* VS-IMSRG (solid line) results. Right: ^{16}C, experiment (symbols) for assumed E_γ energies [see Fig. 3(j) and 3(k)], including the uncertainty from a $\leqslant 13\%$ branching ratio. The solid (dashed) lines show *ab initio* NCSM predictions with (without) 3N interactions. The MBPT results use neutron effective charge $e_n = 0.4$ and g-factors $g_s = -3.55$ and $g_l = -0.09$.

VS-IMSRG transition energies are in very good agreement with experiment, giving 1629 and 2422 keV for the $2_1^+ \rightarrow 0^+$ and $2_2^+ \rightarrow 2_1^+$ decays, respectively. This is at variance with the MBPT results, which overestimate the experimental energies by about 400 keV. The VS-IMSRG $2_2^+ \rightarrow 2_1^+$ partial lifetime in ^{20}O, $\tau = 249$ fs (the solid line), also agrees very well with the present measurement (see Fig. 4). $B(M1) = 0.0166\mu_N^2$ dominates over $B(E2) = 0.0684$ e^2fm^4. The good agreement with the experimental lifetime also suggests a small impact of meson-exchange currents, not included in this calculation.

In $^{10-20}$C isotopes, Forssén *et al.* have performed NCSM calculations with NN + 3N interactions [30]. Like in the VS-IMSRG, total energies and transition probabilities are obtained without effective charges or additional parameters. Consistently with the MBPT calculation on ^{20}O, Forssén *et al.* find the decay rates of the 2_2^+, 3_1^+, and 4_1^+ excited states in ^{16}C sensitive to 3N forces, with transition strengths reduced up to a factor of 7. For the $2_2^+ \rightarrow 2_1^+$ decay, the NCSM finds that the $B(M1) = 0.063\mu_N^2$ dominates, yielding the partial lifetime of $\tau = 81$ fs. Figure 4 shows that the NCSM calculations are consistent with the experimental estimates for transition energy $E_\gamma \geqslant 2216$ keV—this scenario has 78% probability, as discussed above. The absence of a 3980-keV $2_2^+ \rightarrow 0^+$ decay branch in our data, for which we extract an upper limit of 13% (compatible with the previous value of $\leqslant 8.8\%$ [33]), is also consistent with the NCSM NN + 3N results.

Summarizing, we have measured, for the first time, the lifetime of the 2_2^+ state in ^{20}O, and an estimate is given for the 2_2^+ state in ^{16}C. To obtain such results, a novel Monte Carlo technique was developed to determine lifetimes in the tens-to-hundreds of femtoseconds range, using low-energy

transfer and deep-inelastic reactions. This technique will be essential for similar investigations in exotic neutron-rich nuclei produced with intense ISOL-type beams. Crucial in our Rapid Communication was the high precision provided by the AGATA γ-tracking array. The achieved results on transition probabilities agree well with predictions from MBPT and *ab initio* VS-IMSRG for ^{20}O and NCSM calculations for ^{16}C, showing that 3N interactions are needed to accurately describe electromagnetic observables in neutron-rich nuclei. From a broader perspective, the present measurement demonstrates that high-precision γ spectroscopy can benchmark first-principles nuclear structure calculations. This Rapid Communication paves the way toward comprehensive tests of *ab initio* approaches, exploiting electromagnetic transitions in addition to standard comparisons based mostly on nuclear energies.

[1] S. R. Beane, W. Detmold, K. Orginos, and M. J. Savage, Prog. Part. Nucl. Phys. **66**, 1 (2011).

[2] S. Aoki *et al.* (HAL QCD Collaboration), Prog. Theor. Exp. Phys. **2012**, 01A105 (2012).

[3] W. Detmold *et al.* (USQCD Collaboration), Eur. Phys. J. A **55**, 193 (2019).

[4] E. Epelbaum, H. W. Hammer, and U.-G. Meissner, Rev. Mod. Phys. **81**, 1773 (2009).

[5] R. Machleidt and D. R. Entem, Phys. Rep. **503**, 1 (2011).

[6] H.-W. Hammer, A. Nogga, and A. Schwenk, Rev. Mod. Phys. **85**, 197 (2013).

[7] G. Hagen, T. Papenbrock, M. Hjorth-Jensen, and D. J. Dean, Rep. Prog. Phys. **77**, 096302 (2014).

[8] K. Hebeler, J. D. Holt, J. Menéndez, and A. Schwenk, Annu. Rev. Nucl. Part. Sci. **65**, 457 (2015).

[9] P. Navrátil, S. Quaglioni, G. Hupin, C. Romero-Redondo, and A. Calci, Phys. Scr. **91**, 053002 (2016).

[10] D. Lee, Int. J. Mod. Phys. E **25**, 1641010 (2016).

[11] H. Hergert, S. K. Bogner, T. D. Morris, A. Schwenk, and K. Tsukiyama, Phys. Rep. **621**, 165 (2017).

[12] S. R. Stroberg, S. K. Bogner, H. Hergert, and J. D. Holt, Annu. Rev. Nucl. Part. Sci. **69**, 307 (2019).

[13] T. Otsuka, T. Suzuki, J. D. Holt, A. Schwenk, and Y. Akaishi, Phys. Rev. Lett. **105**, 032501 (2010).

[14] F. Wienholtz *et al.*, Nature (London) **498**, 346 (2014).

[15] D. Steppenbeck *et al.*, Nature (London) **502**, 207 (2013).

[16] R. Taniuchi *et al.*, Nature (London) **569**, 53 (2019).

[17] R. F. Garcia-Ruiz *et al.*, Nat. Phys. **12**, 594 (2016).

[18] V. Lapoux, V. Somà, C. Barbieri, H. Hergert, J. D. Holt, and S. R. Stroberg, Phys. Rev. Lett. **117**, 052501 (2016).

[19] P. Gysbers *et al.*, Nat. Phys. **15**, 428 (2019).

[20] A. Kumar, R. Kanungo, A. Calci, P. Navrátil, A. Sanetullaev, M. Alcorta, V. Bildstein, G. Christian, B. Davids *et al.*, Phys. Rev. Lett. **118**, 262502 (2017).

[21] S. Bacca and S. Pastore, J. Phys. G: Nucl. Part. Phys. **41**, 123002 (2014).

[22] F. Raimondi and C. Barbieri, Phys. Rev. C **99**, 054327 (2019).

[23] J. Simonis, S. Bacca, and G. Hagen, Eur. Phys. J. A **55**, 241 (2019).

[24] E. A. McCutchan *et al.*, Phys. Rev. Lett. **103**, 192501 (2009).

[25] E. A. McCutchan *et al.*, Phys. Rev. C **86**, 014312 (2012).

[26] N. M. Parzuchowski, S. R. Stroberg, P. Navrátil, H. Hergert, and S. K. Bogner, Phys. Rev. C **96**, 034324 (2017).

[27] A. B. Garnsworthy *et al.*, Phys. Rev. C **96**, 044329 (2017).

[28] J. Henderson *et al.*, Phys. Lett. B **782**, 468 (2018).

[29] P. Ruotsalainen *et al.*, Phys. Rev. C **99**, 051301(R) (2019).

[30] C. Forssén, R. Roth, and P. Navrátil, J. Phys. G: Nucl. Part. Phys. **40**, 055105 (2013).

[31] M. Wiedeking, S. L. Tabor, J. Pavan, A. Volya, A. L. Aguilar, I. J. Calderin, D. B. Campbell, W. T. Cluff, E. Diffenderfer *et al.*, Phys. Rev. Lett. **94**, 132501 (2005).

[32] M. Wiedeking, P. Fallon, A. O. Macchiavelli, J. Gibelin, M. S. Basunia, R. M. Clark, M. Cromaz, M. A. Deleplanque, S. Gros *et al.*, Phys. Rev. Lett. **100**, 152501 (2008).

[33] M. Petri, S. Paschalis, R. M. Clark, P. Fallon, A. O. Macchiavelli, K. Starosta, T. Baugher, D. Bazin, L. Cartegni *et al.*, Phys. Rev. C **86**, 044329 (2012).

[34] P. Voss, T. Baugher, D. Bazin, R. M. Clark, H. L. Crawford, A. Dewald, P. Fallon, A. Gade, G. F. Grinyer *et al.*, Phys. Rev. C **86**, 011303(R) (2012).

[35] B. Pritychenko, M. Birch, B. Singh, and M. Horoi, At. Data Nucl. Data Tables **107**, 1 (2016).

[36] N. Nakatsuka, H. Baba, T. Aumann, R. Avigo, S. R. Banerjee, A. Bracco, C. Caesar, F. Camera *et al.*, Phys. Lett. B **768**, 387 (2017).

[37] E. Tryggestad, T. Baumann, P. Heckman, and M. Thoennessen, T. Aumann, D. Bazin, Y. Blumenfeld, J. R. Beene *et al.*, Phys. Rev. C **67**, 064309 (2003).

[38] C. Morse, E. A. McCutchan, H. Iwasaki, C. J. Lister, V. M. Bader, D. Bazin, S. Beceiro Novo, P. Chowdhury, A. Gade *et al.*, Phys. Lett. B **780**, 227 (2018).

[39] V. I. Zagrebaev, B. Fornal, S. Leoni, and W. Greiner, Phys. Rev. C **89**, 054608 (2014).

[40] A. V. Karpov and V. V. Saiko, Phys. Rev. C **96**, 024618 (2017).

[41] P. J. Nolan and J. F. Sharpey-Schafer, Rep. Prog. Phys. **42**, 1 (1979).

[42] U. Köster, Eur. Phys. J. A **15**, 255 (2002).

[43] S. Akkoyun *et al.*, Nucl. Instrum. Methods Phys. Res., Sect. A **668**, 26 (2012).

[44] E. Clément *et al.*, Nucl. Instrum. Methods Phys. Res., Sect. A **855**, 1 (2017).

[45] A. Maj *et al.* (PARIS Collaboration), Acta Phys. Pol., B **40**, 565 (2009).

[46] M. Rejmund *et al.*, Nucl. Instrum. Methods Phys. Res., Sect. A **646**, 184 (2011).

[47] S. Pullanhiotan *et al.*, Nucl. Instrum. Methods Phys. Res., Sect. A **593**, 343 (2008).

[48] National Nuclear Data Center, Brookhaven National Laboratory, Upton, NY, https://www.nndc.bnl.gov.

[49] M. Ciemała *et al.* (unpublished).

[50] J. F. Ziegler, J. P. Biersack, and U. Littmark, *The Stopping Power and Range of Ions in Solids* (Pergamon, New York, 1984), Vol. 1.

[51] R. Anne *et al.*, Nucl. Instrum. Methods Phys. Res., Sect. B **34**, 295 (1988).

[52] C. Broude, U. Karfunkel, and Y. Wolfson, Nucl. Phys. A **161**, 241 (1971).

[53] F. Hibou, P. Fintz, B. Rastegar, and A. Gallmann, Nucl. Phys. A **171**, 603 (1971).

[54] R. Venturelli and D. Bazzacco, LNL Annual Report No. 2004, https://www.lnl.infn.it/~annrep/read_ar/2004/index_2004.html.

[55] B. Bruyneel, B. Birkenbach, and P. Reiter, Eur. Phys. J. A **52**, 70 (2016).

[56] A. Lopez-Martens, K. Hauschild, A. Korichi, J. Roccaz, and J.-P. Thibaud, Nucl. Instrum. Methods Phys. Res., Sect. A **533**, 454 (2004).

[57] D. R. Entem and R. Machleidt, Phys. Rev. C **68**, 041001(R) (2003); J. Simonis, K. Hebeler, J. D. Holt, J. Menendez, and A. Schwenk, *ibid.* **93**, 011302(R) (2016).

[58] R. F. Garcia Ruiz *et al.*, Phys. Rev. C **91**, 041304(R) (2015).

[59] A. Klose, K. Minamisono, A. J. Miller, B. A. Brown, D. Garand, J. D. Holt, J. D. Lantis, Y. Liu *et al.*, Phys. Rev. C **99**, 061301(R) (2019).

[60] E. Caurier, G. Martínez-Pinedo, F. Nowacki, A. Poves, and A. P. Zuker, Rev. Mod. Phys. **77**, 427 (2005).

[61] K. Tsukiyama, S. K. Bogner, and A. Schwenk, Phys. Rev. C **85**, 061304(R) (2012).

[62] S. R. Stroberg, H. Hergert, J. D. Holt, S. K. Bogner, and A. Schwenk, Phys. Rev. C **93**, 051301(R) (2016).

[63] S. R. Stroberg, A. Calci, H. Hergert, J. D. Holt, S. K. Bogner, R. Roth, and A. Schwenk, Phys. Rev. Lett. **118**, 032502 (2017).

[64] J. Simonis, S. R. Stroberg, K. Hebeler, J. D. Holt, and A. Schwenk, Phys. Rev. C **96**, 014303 (2017).

[65] T. D. Morris, N. M. Parzuchowski, and S. K. Bogner, Phys. Rev. C **92**, 034331 (2015).